Scientific Journals
of the Maritime University of Szczecin

Zeszyty Naukowe
Akademii Morskiej w Szczecinie

2019, 58 (130), 45–54
ISSN 1733-8670 (Printed)
ISSN 2392-0378 (Online)
DOI: 10.17402/335

Received: 10.05.2019
Accepted: 17.06.2019
Published: 25.06.2019

Analysis of the accuracy of shoreline mapping in inland navigational charts (Inland ENC) using photogrammetric and sonar images

Jacek Łubczonek✉, Małgorzata Łącka, Grzegorz Zaniewicz

Maritime University of Szczecin, Faculty of Navigation, Institute of Geoinformatics
146 Żołnierska St., 71-250 Szczecin, Poland
e-mail: {j.lubczonek; m.lacka; g.zaniewicz}@am.szczecin.pl
✉ corresponding author

Key words: photogrammetry, navigation chart, hydrography, side scan sonar, accuracy assessment, mapping

Abstract
Shoreline mapping is one of the key stages in navigational charting. In terms of navigation, the shoreline marks the boundary of a river, which is often equivalent to the navigable water area. In cartographic terms, it is an important topological element between different objects that are adjacent to it. Currently, topographic objects are often mapped using photogrammetric materials obtained from various altitudes – satellite, airborne or low, which is associated with the use of an airborne UAV. Depending on the type of materials, the shoreline can be obtained in vector form with differing situational accuracy and differing degree of detail. In addition to the standard methods of processing vector data, the research in this paper also included the use of sonar images, enabling the detection of the shoreline with the use of a surveying hydrographic unit. On the basis of the collected photogrammetric and sonar images of different spatial resolution, an analysis of the accuracy of shoreline mapping was performed in terms of the situational accuracy and the level of detail in its representation. The results of the research provided the basis for the determination of dedicated remote sensing materials enabling the development of maps for inland navigation.

Introduction

The shoreline is one of the basic elements of numerical maps. Regardless of whether they are topographic, general geographic or navigational maps, the shoreline marks the border of the land and water areas, which include oceans, seas, lakes and watercourses. In inland navigational charts (Inland ENC), the shoreline is particularly important because it often marks the boundaries of navigational water areas. Other applications include the analysis of coastal line changes caused by the impact of water masses on land areas, which makes it possible to keep track of changes occurring in coastal zones of sea or inland waters. The need for shoreline mapping also implies the development of new methods for its determination (Liu et al., 2017; Dominici et al., 2019). The process of geodata acquisition has changed over the years. Nowadays, numerical maps are created, including the geometric and descriptive geographical feature parts, so the shoreline is already in digital form. This is also the form of the data from which the shoreline is obtained, and these are all kinds of orthoimages that are obtained from satellite or airplane altitudes. The diversity of the sensors, such as sensors imaging in the range of visible radiation, microwaves (radar images) and LIDAR data, should also be mentioned here.

Nowadays, low altitude photogrammetry is particularly important. Using increasingly perfect UAV platforms it is possible to obtain blocks consisting of up to 150,000 photos, in measurement campaigns lasting up to several dozen days. The fundamental question to be answered concerns the accuracy

with which the shoreline can be mapped and what problems should be expected. Taking into account previous experience and studies in creating electronic maps for navigation (Łubczonek & Włodarczyk, 2010) and similar studies (Wilkowski et al., 2017; Templin, Popielarczyk & Kosecki, 2018), the research has been extended to include the possibility of using sonar images. The motivation for this approach was to increase the possibilities for shoreline mapping. This is due to frequent difficulties in the identification of the shoreline, which is caused by the presence of vegetation growing along the banks of rivers as well as vegetation in the water. It is also worth mentioning that the assessment of the usefulness of the image data in determining the shoreline enables further implementation and development of methods for their automatic extraction (Łubczonek, 2016; Paravolidakis et al., 2018).

Due to the high availability of data and the possibility of obtaining data in order to map the shoreline, this study was conducted to evaluate the use of the data in the creation of electronic databases of navigational maps. The research was conducted with the use of sonar and photogrammetric images, such as satellite, aerial and low altitude UAV images.

Selected data acquisition methods

Sonar imaging methods

Underwater sonar imaging is based on the principles of underwater acoustics. These devices are becoming more and more sensitive and can, depending on the system, visualize elements smaller than 10 cm on the sea bottom. Typical applications for sonar include: object detection (i.e. mines, shipwrecks and other sunken vehicles, underwater pipelines, lost cargo), seabed classification (i.e. types of sediment, rock formations, ripplemark structures) and underwater structural inspections (i.e. bridges, pylons, quay walls and mining infrastructure). Side scan sonar is towed behind the measurement boat or is hull mounted. The device emits an acoustic signal in the form of pulses perpendicular to the direction of movement of the head. The mounted sensitive receivers (also called hydrophones) receive the reflected signal and it is processed into a digital image. Returning echoes from a single pulse are presented as a single line with light and shades of colour, representing weak or strong reflections relative to the transient time of the acoustic pulse (Lekkerkerk & Theijs, 2011).

Modern towed sonar usually operate at two frequencies: low and high, for example: 100/500 kHz, 600/1600 kHz. Generally, high frequency is used where high image resolution is required, but its range is limited. A lower sonar frequency provides a lower resolution image but, thanks to the higher power of the acoustic signal, has the capability of a larger search range. As the pulse sent from the sonar reaches the surface of the bottom or an object at the bottom, it is possible that the material may absorb the signal or disperse it, backscatter it or mirror it. All the above mentioned acoustic reflections depend on the material and the topography of the imaging area and affect the content of the image in the final phase (Mazel, 1985).

Photogrammetric imaging methods

The most common photogrammetric product is an orthophotomap, i.e. a product based on aerial photographs or satellite images. This is due to the entry into the market of aerial digital cameras and automated image processing. Currently information can be found on the Polish Geoportal website (www.geoportal.gov.pl) in index tables about the validity of the orthophotomap and its spatial resolution. Additionally, it is also possible to obtain information on where further orthophotomaps are planned to be developed and on what stage of production advancement they are currently in (in progress, planned).

The quality of an orthophotomap as a final product is measured by the errors that occur at earlier production stages, such as: aerial photography (occurrence of clouds, shadows, snow, blurred photos), aerotriangulation, DTM measurement (e.g. no separation of engineering objects such as viaducts or bridges), and orthophotomap generation related to the geometry and radiometry of the image (Karwel, 2012).

A satellite orthophotomap with a resolution of 1 m and an aerial orthophotomap with a resolution of 0.5 m were used to map the shoreline for navigation purposes (Stateczny & Łubczonek, 2011). This spatial resolution was sufficient and the solution resulted in time-savings. In the case of objects that are important for navigation, such as bridges, the orthotophotomap proved to be insufficient due to errors caused by shifts, so it was necessary to perform additional GNSS-RTK measurements. Increasing the resolution of the orthophotomap may be important for the acquisition of data for navigation purposes.

The appearance of Unmanned Aerial Vehicles (UAV) on the market and their use in photogrammetric purposes resulted in a change in the perception of the orthophotomap as a product. In the literature, acronyms can be found such as UAS (Unmanned Aircraft System), as well as more informal terms such as: drone or unmanned aerial vehicle in the current terminology, these terms mean "a flying structure that carries out a flight without a pilot on board, has no possibility to take passengers and allows for multiple use" (Sawicki, 2012). The multicopter type is especially popular in photogrammetric works, because they proved the possibility of vertical take-off and landing, as well as hovering (Burdziakowski, 2016). Also worth mentioning is the development of new multi-camera imaging systems that allow for more accurate and complete data acquisition (Wierzbicki, 2018). For photogrammetric purposes, micro- or mini-types of UAS are most often used and their characteristic feature is low weight and light payload, and their working time in the air does not exceed 2 hours (Colomina & Molina, 2014). Drones turned out to be irreplaceable for imaging small areas where a fast data acquisition time and high field resolution are important (Kędzierski, Fryśkowska & Wierzbicki, 2014). Acquisition techniques for photogrammetric data are also being constantly studied and include various parameters relating to the recording of an image e.g. radiometry (Wierzbicki et al., 2018). So in the short term, UAS sensors can be improved and can provide high quality photogrammetric products.

UAVs currently have a very wide range of civilian applications. They are used, among others, in the industrial sector, in agriculture and forestry, in marketing, rescue and environmental monitoring, including the inventory of cliff banks and water reservoirs (Čermakova, Komárková & Sedlak, 2016; Templin, Popielarczyk & Kosecki, 2018).

Data acquisition

Sonar Images

For the purpose of verifying the thesis of this article on the use of sonar data for mapping the shoreline, the authors decided to prepare real data collected in the defined area of the Szczecin harbour. The hydrography and research boat Hydrograf XXI, which is a floating laboratory for the students and scientists of the Maritime Academy in Szczecin, was used in the tests. The measurement set consisted of a dual frequency Edgetech 4125 towed side scan sonar, a GNSS-RTK positioning system and a computer with sonar data acquisition software.

Data acquisition was carried out in fixed installation sonar mode, which allowed the antenna of the positioning system to be mounted directly above the sensor, which resulted in a significant increase in positioning accuracy, unlike the layback method for towed sonar mode (Figure 1). The accuracy of data acquisition for shoreline mapping is a very important issue.

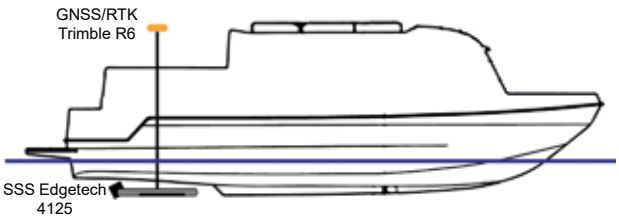

Figure 1. Diagram of the side scan sonar survey system

The test tracklines ran along both reinforced (concrete) and undefined (green) quays. The data were recorded at two sonar acoustic frequencies, at ranges of 25 and 50 m and GNSS-RTK positioning accuracy was used. The average survey speed was 2–3 kn. During the data acquisition process, 18 sonar data files were recorded, from which representative data were selected to verify the accuracy of the method.

Processing of sonar images can be divided into several main stages, which in dedicated hydrographic software occur independently of the manufacturer. The following diagram (Figure 2) shows the process from loading to creating a geo-referencing product called a sonar mosaic.

The data processing begins with the import of the sonar data. The software processes the raw data into files to be edited (the raw data remains unchanged). In the first step, the first reflection from the bottom is indicated. This distance also determines the height of the towed sonar above the bottom. As a result of this process, the dead zone is eliminated and slant range correction is applied. The apparent position of the pixels in close proximity to the sonar is mapped

Figure 2. Scheme for sonar data processing

to the correct position due to the reflection time of the beam and the height of the sonar above the bottom (Blondel & Murton, 1997).

After geometric correction of the image, the signal is processed. After applying all available tools, the image should be normalized in terms of its intensity while maintaining its details, e.g. elements lying at the bottom (Łubczonek & Zaniewicz, 2013). For the purposes of this article, the authors used Hypack software, which has several tools for signal processing, including Automatic Gain Control, Auto Time Varying Gain and manual settings.

In the last stage, a sonar mosaic was generated, which is a geo-referenced product ready for the vectorization of the discussed shoreline. A minimum pixel size of 8 cm was applied. Vectorization was performed in the ArcMap application of the ArcGIS package (Figure 3).

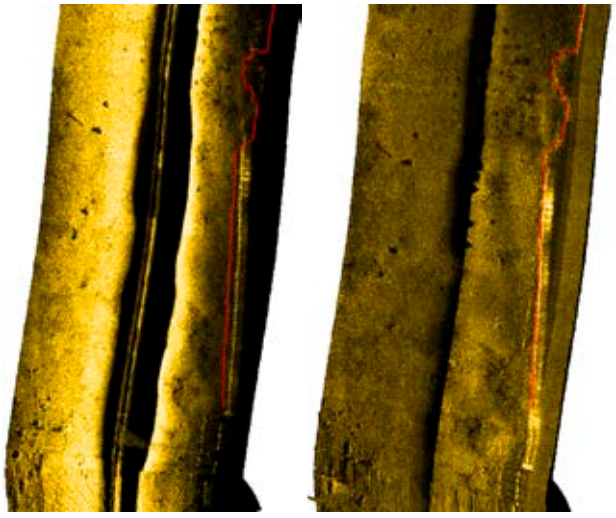

Figure 3. Sonar image before (left) and after (right) application of geometric correction and image filtration (red line represents shoreline)

Satellite and aerial orthoimagery

The following photogrammetric materials were used in the research: satellite images with a resolution of 100 cm, aerial orthoimages with resolutions of 50 cm and 15 cm and also orthomosaics with a resolution of 2.6 cm obtained from a low altitude flight.

Ikonos was the first commercial satellite built by the Lockheed company, which imaged with a spatial resolution at nadir of 0.82 m in the panchromatic channel and 3.28 m in the multi-spectral range. It was launched in 1999 and its mission ended in March 2015. It moved in a heliosynchronous orbit. Currently, the data is owned by Digital Globe, previously the satellite was owned by GeoEye. A single scene has a size of 11×11 km^2.

The orthophotomap was created with the use of colour aerial photographs with 50 cm field pixels, which were taken in 2007 with the use of the DMC camera from Intergraph. The orthophotomap was developed using DTM in the TIN structure and elements of external orientation of the photos were determined within the framework of the aerotriangulation. The control of the geometric accuracy of the orthophotomap showed an average error of 10 cm.

An orthophotomap with a resolution of 15 cm was prepared on the basis of aerial photographs obtained with the DMC II digital camera in April 2013. Apart from the standard R-red, G-green and B-blue channels, the aerial photographs were also obtained in the near-infrared channel, which allowed an orthophotomap to be produced not only in natural colours but also in spectro-zone composition.

Low altitude orthomosaic

The data for the orthomosaic was obtained on 13.10.2018 using a DJI Unmanned Aerial System – Phantom 4 Pro. The flight took place at an altitude of 100 m. During the flight 310 photos were taken, which covered the area of the study of about 12.6 ha. GCP (Ground Control Points) were previously measured on the photographed area by the GNSS-RTK method in the TPI NETpro network with maximum errors in the position of a point of 0.01 m (mp, mh). The photographs were developed in Pix4D software and as a final product an orthophotomap with a spatial resolution of 2.6 cm was created. A view of the centres of the photos on the background of the elaborated orthomosaic is illustrated in Figure 4.

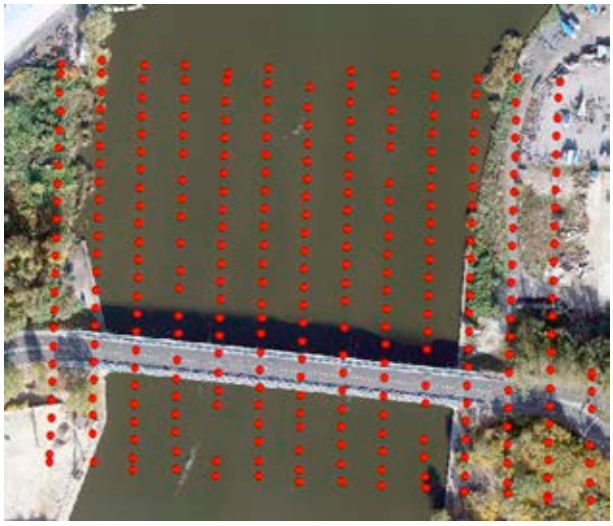

Figure 4. View of the centres of the photos on the background of the orthomosaic

Shoreline mapping and accuracy analysis

The near vicinity of the Cłowy Bridge on Szczecin's right bank, located on the Eastern Oder (Regalica) near Lake Dabie, was selected as the area for the research analysis. The location was selected for the two types of shoreline (concrete and natural) that occur in the area. To the south of the bridge, the shoreline on the right and left side of the river was mapped out to a distance of about 100 metres, where there is mainly a concrete shoreline. To the north of the bridge an area of 200 metres on each side of the shore was mapped out. The only exception was the sonar survey, which did not cover the left shoreline on the south side of the bridge. A list of vectorised lines is presented in Figures 5 and 6.

Shoreline mapping was performed in the ArcMap software in the PUWG 1992 coordinate system. Each of the materials was vectorised independently so that the edge lines that were obtained were valuable material for comparative analysis. The most difficult, from the interpretation point of view, were the places with dense vegetation (low and high), which

Figure 6. Vectorised lines from sonar mosaic

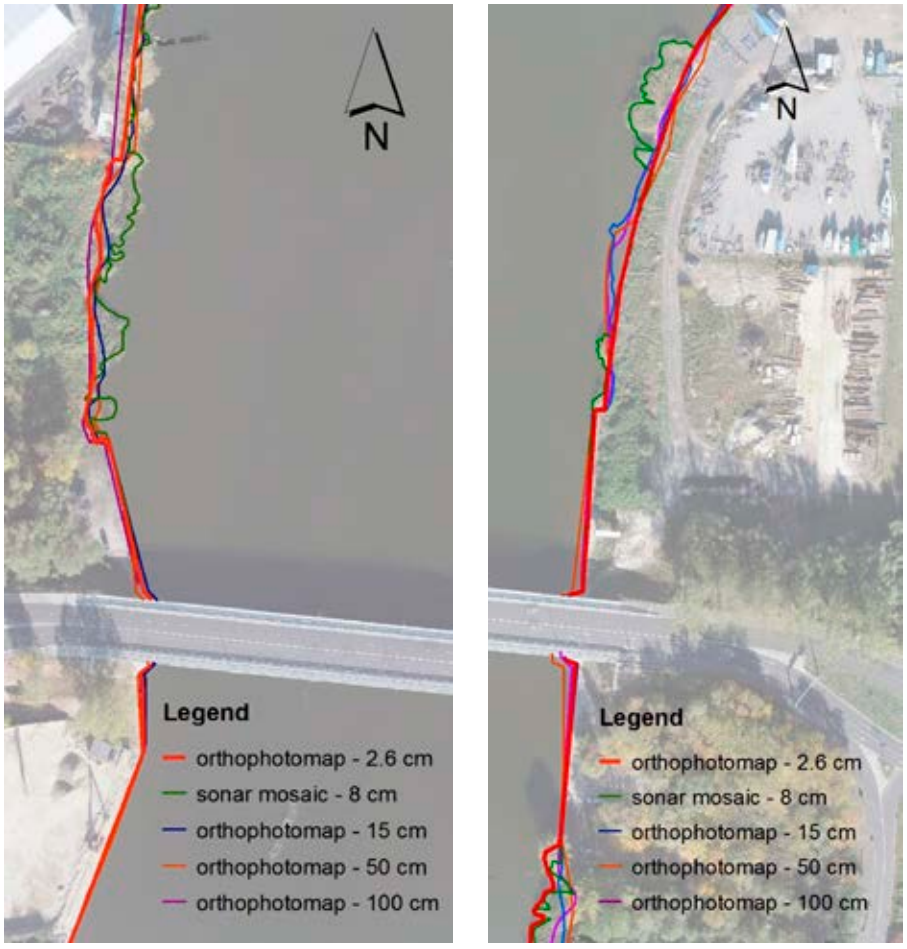

Figure 5. Vectorised lines from photogrammetric materials (left and right edge)

made it impossible to identify the shoreline in a certain way. The most accurate and time-consuming material for manual digitization was an orthophotomap with a resolution of 2.6 cm.

Accuracy analysis was performed in ArcGIS (Esri Geographic Information System) using the Digital Shoreline Analysis System (DSAS) add-in to Esri's ArcGIS (Himmelstoss et al. 2018). The idea of this add-in is to compare the edge lines (one or more) to a user selected base line (the one from which any deviation is calculated). The work with the DSAS add-in requires initial preparation of the data for further processing. All input and output data are stored in a geodatabase. The parameters for analysis, such as base line selection, boundary line selection, maximum boundary line distance, intersection line distance (so-called transects), can be set individually for each processing. An example of an analysis of a shoreline vectorised from a sonar mosaic and photogrammetric images with a resolution of 50 cm and 2.6 cm using transects is illustrated in Figure 7.

Two approaches have been adopted for the analysis of the shoreline. In the first one, the base line was based on the orthophotomap from the UAS flight (2.6 cm). Next, the shoreline's deviation obtained from all the image data were compared to the selected baseline. The obtained results are summarized in the tables below (Tables 1 and 2). The analysis was conducted independently for the right and left shorelines and they included part of the natural line and the concrete bank.

The results for the left edge are comparable to the mean, minimum and maximum deviations for the 15 cm and 50 cm resolution images. Slightly larger deviation occurred for images with a resolution of 100 cm, especially in the range of the standard deviation and maximum deviation. The sonar mosaic, for which the deviation was almost three times lager, was much worse. For the right bank the biggest deviation occurred for the 50 cm resolution images and the sonar mosaics. Overall, the best results were achieved for the 15 cm orthophotomap, while the greatest discrepancies were found for the sonar mosaic.

The second approach was to survey the concrete bank. The base line is the line developed from the

Figure 7. Transects between the sonar image and the orthoimage of 2.6 cm (left) and 50 cm (right)

GNSS-RTK measurements, to which the other lines derived from the image data were compared. The results of the analyses are summarized in Tables 3 and 4. The analysis was carried out separately for the right and left banks.

In this case, the results are quite different. First of all, there was a significant decrease in all types of deviation. The value of 1 m for both the maximum and mean values was only exceeded for the orthophotomap with 50 cm resolution. The best results were obtained for the orthophotomap with a resolution of 2.6 cm and a mean value of 2–4 cm. Higher values were observed for the 15 cm resolution orthophotomap, ranging from 0.28 to 0.52 m. Quite good results were achieved with the use of the sonar mosaic (mean deviation 0.32–0.38 m). The mean values for the 100 cm and 50 cm orthophotomaps were 0.52–0.71 m and 0.66–1.52 m, respectively.

Table 1. Comparative analysis for the left bank (baseline – UAS orthophotomap)

Statistics	Orthophoto			Sonar mosaic 8 cm
	15 cm	50 cm	100 cm	
MIN [m]	0.003	0.007	0.0003	0.13
MAX [m]	4.62	4.19	5.21	12.04
MEAN [m]	1.21	1.20	1.38	3.65
Standard Deviation [m]	1.06	1.03	1.54	3.81
COUNT	307	302	298	189

Table 2. Comparative analysis for the right bank (baseline – UAS orthophotomap)

Statistics	Orthophoto			Sonar mosaic 8 cm
	15 cm	50 cm	100 cm	
MIN [m]	0.003	0.005	0.032	0.002
MAX [m]	10.62	12.48	10.79	12.52
MEAN [m]	1.88	2.98	2.12	2.07
Standard Deviation [m]	2.58	2.94	2.35	3.27
COUNT	319	318	315	293

Table 3. Comparative analysis for the left shoreline (baseline – GNSS-RTK measurement)

Statistics	Orthophoto				Sonar mosaic 8 cm
	2.6 cm	15 cm	50 cm	100 cm	
MIN [m]	0.0001	0.001	0.009	0.005	0.25
MAX [m]	0.09	1.53	2.25	1.21	0.49
MEAN [m]	0.04	0.52	0.66	0.52	0.38
Standard Deviation [m]	0.02	0.44	0.44	0.45	0.07
COUNT	142	144	136	139	41

Table 4. Comparative analysis for the right shoreline (baseline – GNSS-RTK measurement)

Statistics	Orthophoto				Sonar mosaic 8 cm
	2.6 cm	15 cm	50 cm	100 cm	
MIN [m]	0.00002	0.002	0.001	0.075	0.015
MAX [m]	0.18	0.70	3.68	1.15	0.83
MEAN [m]	0.02	0.28	1.52	0.71	0.32
Standard Deviation [m]	0.03	0.20	0.92	0.22	0.23
COUNT	103	105	103	105	87

Due to the discrepancies in the accuracy of the edge line mapping in the two cases studied, fragments of the places with the maximum deviation were additionally analysed. The analysed cases concerned the areas with aquatic vegetation, tree crowns and concrete banks.

The aquatic vegetation grows partly on the banks of the river, so it is important to identify it and distinguish it from the actual shoreline. In the case of photogrammetric images with a lower resolution, it is difficult to clearly distinguish between the land and the water. Considerably better results can be achieved by using low altitude images, which, being high resolution, enable much better identification of water vegetation, and thus, the identification of the shoreline. In images of 100 cm or even 50 cm resolution, the main criterion for vectorization is the colour difference between the water and the land. The colour of surface vegetation is often indistinguishable from the colour of coastal vegetation, which can result in incorrect vectorization of the shoreline. Examples of the maximum deviation related to the shoreline obtained from a UAS orthophoto are given in Figure 8.

Another case concerned trees in the vicinity of the shoreline. In the area of the natural shoreline, there are often trees whose crowns make it very difficult to correctly identify the shoreline. High-resolution images provide better interpretations and, even when trees are present, correct identification as well as vectorization of the shoreline is possible. Images with a worse terrain pixel can cause the crown line (seen from above on an orthophotomap) to be mistakenly drawn as a shoreline. In order to further reduce the negative effects of shoreline delineation caused by tree crowns, the time of flight can be adjusted according to the vegetation period of the vegetation. On the following drawings (Figure 9) it can be seen that the vectorization of the shoreline on orthophotomaps, regardless of the size of the terrain pixel, is much worse than the vectorization on the

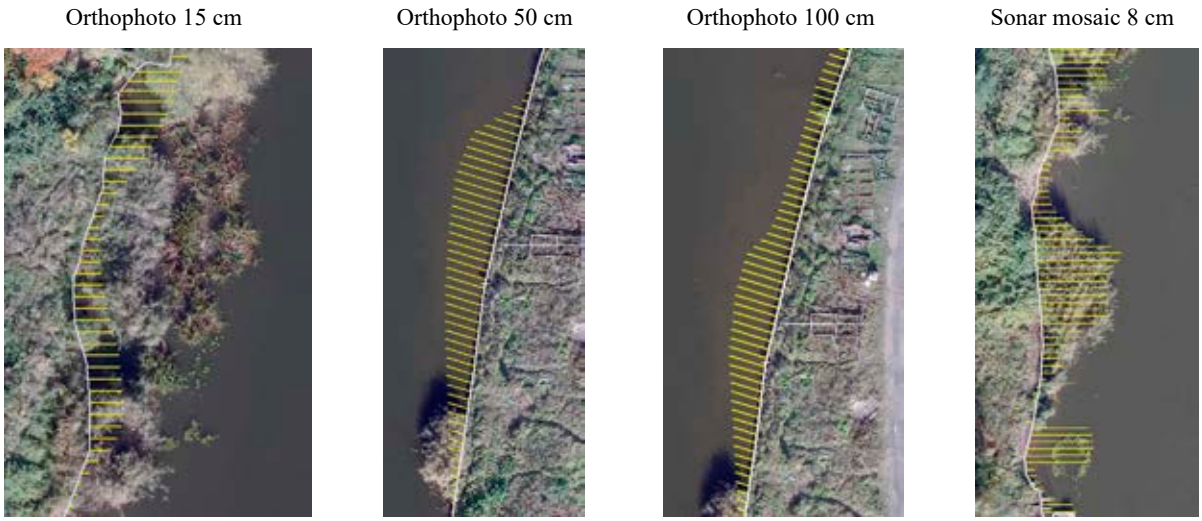

Figure 8. Areas with the greatest deviations – the case of aquatic vegetation

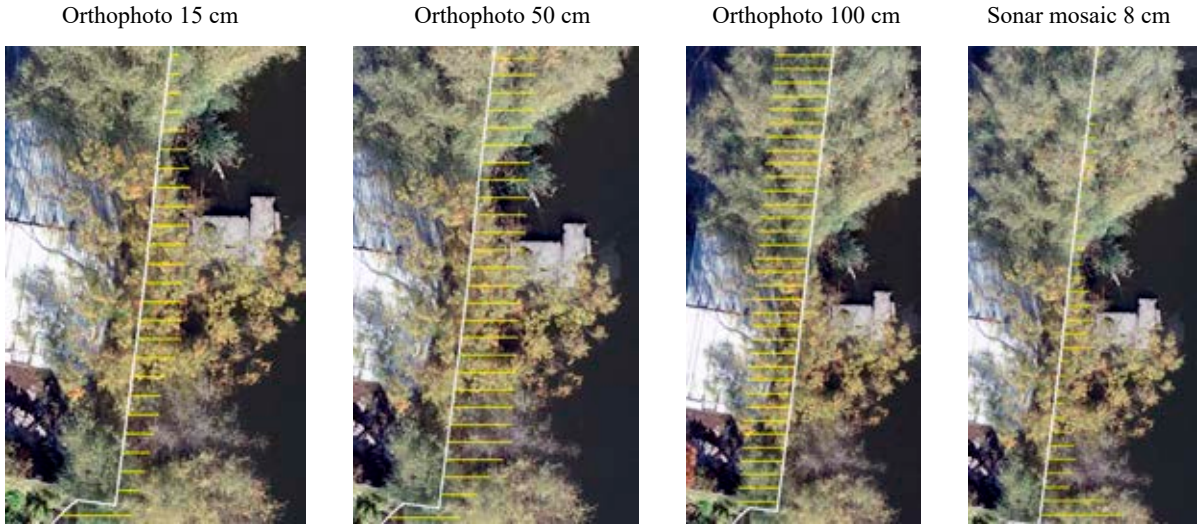

Figure 9. Summary of areas with the greatest deviation – crown case

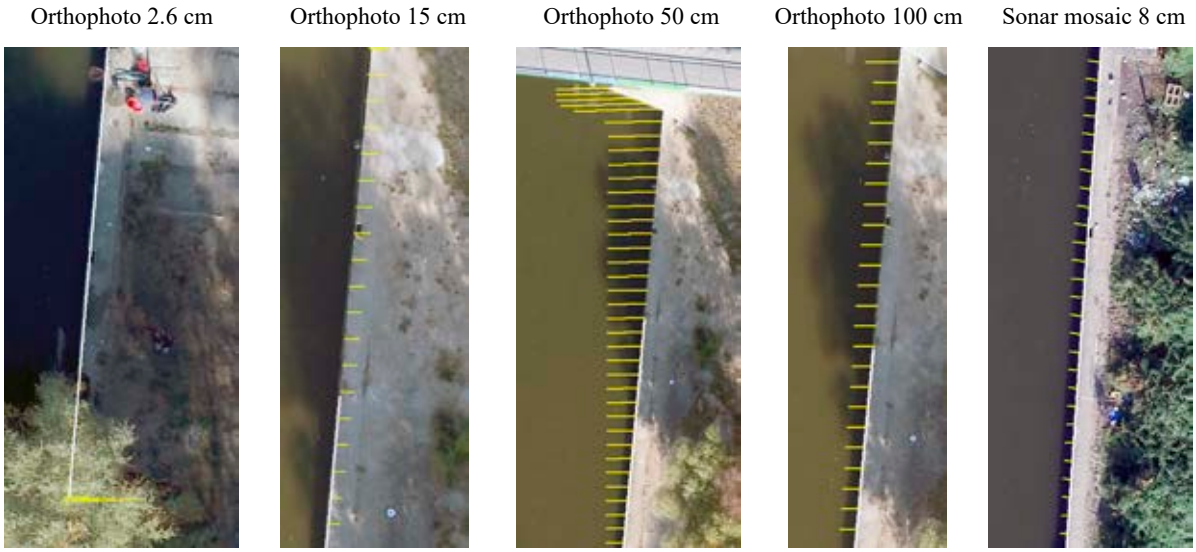

Figure 10. Summary of the most deviated areas – concrete shoreline

sonar mosaic, where the crowns of the trees did not affect the accuracy of the shoreline determination.

Concrete shoreline (hardened) is unambiguous in its identification and its vectorization is much simpler compared to the natural shoreline. The GNSS-RTK method was used as a reference measurement for the concrete shoreline. The mean difference between the GNSS-RTK and the 2.6 cm orthophotomap was only 4 cm for the left bank and 2 cm for the right bank. The biggest deviation occurred in the corner covered with the crown of a tree, where the difference between the measurements was 18 cm. The sonar measurement also gave relatively good results. Large errors that occur on 15 cm and 50 cm orthophotomaps result from the total shift of the shoreline in relation to other measurements, which can be caused by geometric errors in the orthophotomap. Selected cases of deviation from the RTK measurement are illustrated in Figure 10.

From analysing sonar images it can be stated that the biggest problem is bottom levelling in shallow water bodies. Greater differences between the data result from the specific properties of the side scan sonar data acquisition. Due to the side characteristics of the generated acoustic beam, the acoustic signal is received at the first incidence on the slope of the examined unfortified quay and there is no possibility of it reaching the meeting point of the land line with the water. Examples of differences between the shoreline from the UAV and the sonar images are illustrated in Figure 11.

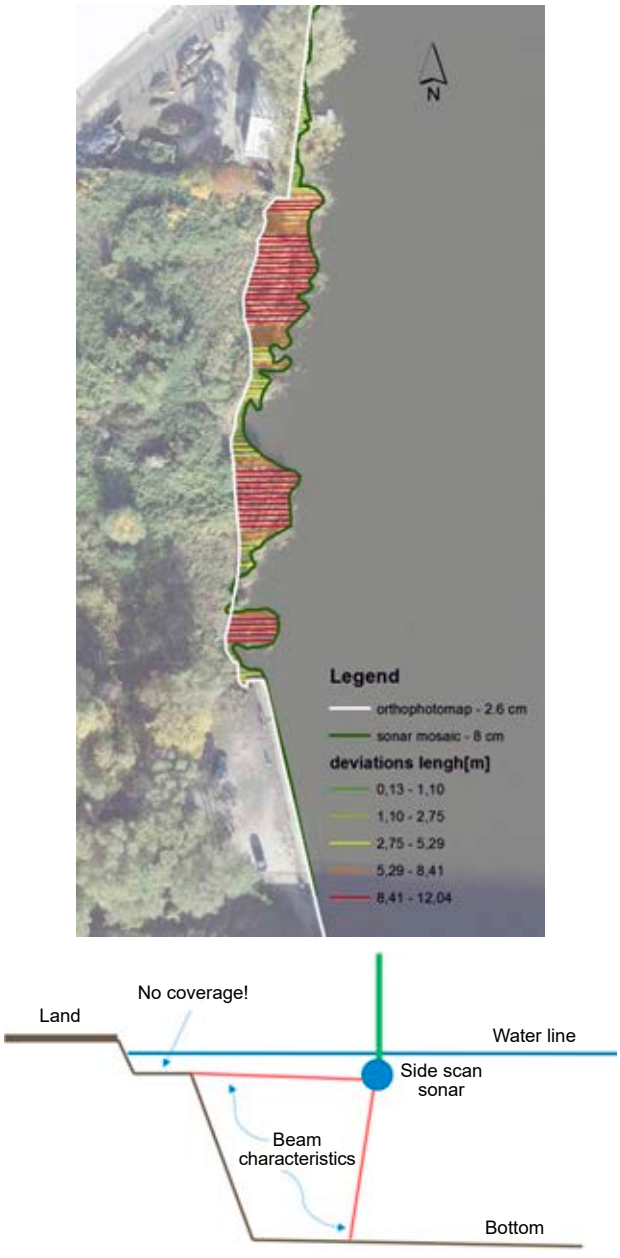

Figure 11. Deviation between the UAS and sonar measurement line and bottom levelling case diagram

Conclusions

On the basis of the research conducted it can be stated that the biggest factor that influences the accuracy of shoreline mapping is its type. The objects that generate most of the errors are the vegetation growing along the banks of the river, including trees. In the case of the image type, the best choice is to use low altitude images. They definitely contain the fewest errors, which is due to the local distribution of the checkpoints used to develop the orthomosaics. Another advantage of this type of study is very good resolution, which allows the land part to be distinguish from the water, and thus provide correct identification of the shoreline. In the case of a large study area (orthophotomaps and satellite scenes), larger errors may be caused by the lower spatial resolution and larger errors in the development of the photogrammetric material (alignment of the block of photos). An objective comparison of the mapped shoreline can be made on a concrete section of the shoreline where the best results were obtained for the product from the UAV flight. The mean value of the deviation on the examined fragment was 4 cm for the left quay and 2 cm for the right quay. Relatively large errors of the orthophotomaps with a resolution of 15 cm and 50 cm were caused by the shift of the shoreline on the whole worked out sheets.

Interesting results were observed for the sonar images; the use of sonar data as a source of data for shoreline mapping seems to be a very good method of supplementing conventional methods used in previous work. The data obtained by the sonar method certainly differed from the data collected by photogrammetry. The advantage of using sonar images is

the possibility of verifying the shoreline under the crowns of trees, even during a period of increased vegetation and in places where classical measurement is impossible. However, their use for the final mapping of the shoreline is rather limited to concrete banks.

Acknowledgments

This research outcome has been achieved under the grant No. 19/MN/IG/18 and 1/S/IG/16 financed from a subsidy of the Ministry of Science and Higher Education for statutory activities.

References

1. Blondel, P. & Murton, B.J. (1997) *Handbook of seafloor sonar imagery*. Chichester – New York – Weinheim – Brisbane – Singapore – Toronto: John Wiley & Sons.
2. Burdziakowski, P. (2016) Review of construction and functionality of photogrammetric unmanned aerial vehicles. *Biuletyn WAT* LXV, 4 (in Polish).
3. Čermáková, I., Komárková, J. & Sedlak, P. (2016). *Using UAV to detect shoreline changes: case study – Pohranov Pond, Czech Republic*. The International Archives of the Photogrammetry, Remote Sensing and Spatial Information Sciences, Volume XLI-B1, XXIII ISPRS Congres, 12–19 July 2016, Prague, Czech Republic, pp. 803–808. 10.5194/isprsarchives-XLI-B1-803-2016.
4. Colomina, I. & Molina, P. (2014) Unmanned aerial systems for photogrammetry and remote sensing: A review. *ISPRS Journal of Photogrammetry and Remote Sensing* 92, pp. 79–97.
5. Dominici, D., Zollini, S., Alicandro, M., Della Torre, F., Buscema, P. & Baiocchi, V. (2019) High Resolution Satellite Images for Instantaneous Shoreline Extraction Using New Enhancement Algorithms. *Geosciences* 9 (3), 123, doi: 10.3390/geosciences9030123.
6. Karwel, K. (2012) Influence initial data for quality of aerial photogrammetry products, Archives of Photogrammetry. *Cartography and Remote Sensing* 24, pp. 123–132 (in Polish)
7. Kędzierski, M., Fryśkowska, A. & Wierzbicki, D. (2014) *Photogrammetric elaboration from a low altitude*. Warsaw: Military University of Technology (in Polish).
8. Lekkerkerk, H-J. & Theijs, M.J. (2011) *Handbook of offshore surveying*. Oil Pub – Skill Trade.
9. Liu, Y., Wang, X, Ling, F., Xu, S. & Wang, Ch. (2017) Analysis of Coastline Extraction from Landsat-8 OLI Imagery. *Water* 9(11), 816, doi: 10.3390/w9110816.
10. Łubczonek, J. (2016) Geoprocessing of High Resolution Imageries for Shoreline Extraction in the Process of the Production of Inland Electronic Navigation Charts. *Photogrammetrie-Fernerkundung-Geoinformation* 4, pp. 225–235.
11. Łubczonek, J. & Włodarczyk, M. (2010) Charting of the shoreline of inland waters using digital remote sensing images. *Scientific Journals of the Maritime University of Szczecin, Zeszyty Naukowe Akademii Morskiej w Szczecinie* 22 (94), pp. 53–58.
12. Łubczonek, J. & Zaniewicz, G. (2013) Analysis of selected methods for enhancing the content of sonar images. *Annals of Geomatics* 11(2 (59)), pp. 59–68 (in Polish).
13. Mazel, Ch. (1985) *Side Scan Sonar Record Interpretation*. Klein Associates Inc.,
14. Paravolidakis, V., Ragia, L., Moirogiorgou, K. & Zervakis, M.E. (2018) Automatic Coastline Extraction Using Edge Detection and Optimization Procedures. *Geosciences* 8 (11), 407, doi: 10.3390/geosciences8110407.
15. Sawicki, P. (2012) Unmanned aerial vehicles in photogrammetry and remote sensing – state of the art and trends. *Archives of Photogrammetry, Cartography and Remote Sensing* 23, pp. 365–376 (in Polish)
16. Stateczny, A. & Łubczonek, J. (2011) Selected aspects of the elaboration, verification and implementation of inland electronic charts for RIS area in Poland. *Logistyka* 6.
17. Templin, T., Popielarczyk, D. & Kosecki, R. (2018) Application of Low-Cost Fixed-Wing UAV for Inland Lakes Shoreline Investigation. *Pure and Applied Geophysics* 175, 9, pp. 3263-3283.
18. Wierzbicki, D. (2018) Multi-Camera Imaging System for UAV Photogrammetry. *Sensors* 18 (8), 2433, doi: 10.3390/s18082433.
19. Wierzbicki, D., Fryśkowska, A., Kędzierski, M., Wojtkowska, M. & Deliś, P. (2018) Method of radiometric quality assessment of NIR images acquired with a custom sensor mounted on an unmanned aerial vehicle. *Journal of Applied Remote Sensing* 12 (1), doi: 10.1117/1.JRS.2.015008.
20. Wilkowski, W., Lisowski, M., Wyszyński, M. & Wierzbicki, D. (2017) The use of unmanned aerial vehicles (drones) to determine the shoreline of natural watercourses. *Journal of Water and Land Development* 35 (X–XII), pp. 259–264.